Supporting Information

Supplementary Figure Legends

Supplementary Figure S1. Full-length, inactive human vinculin does not bind to the RRM motifs of raver1

Isothermal titration calorimetry results of human vinculin and (**A**) RRM1-3 or (**B**) RRM1 are shown. Binding of Vt to raver1 is seen (**C**), but no binding is seen for full-length vinculin (**D**) by size exclusion chromatography and SDS-PAGE.

Supplementary Figure S2. Stereo view of the Vt:RRM1-3 and Vt:RRM1 complex structures

(**A**) Stereo Cα-trace of the Vt:RRM1-3 complex (Vt, green and raver1 domains in blue, RRM1, yellow, RRM2, and red, RRM3). Residues comprising the RNP1 and RNP2 motifs in each RRM domain are shown. (**B**) Stereo view of the final $2F_o$-F_c electron density map of the RNP1 and RNP2 sites of RRM1 (residues 61-66 and 93-100) as seen in the 2.9Å Vt:RRM1 structure, and (**C**) RRM2 (residues 134-139 and 173-180) and **(D***)* RRM3 (residues 223-228 and 262-269) as seen in the 2.75 Å Vt:RRM1-3 structure, contoured at 1σ.

Supplementary Figure S3. Superposition of the Vt:RRM1 and Vt:RRM1-3 structures

(**A**) The structure of the human vinculin tail (residues 879–1066; light green) when bound to RRM1 versus when bound to the RRM1-3 domains (yellow). Vt helices H1–H5 correspond to those present in human vinculin (PDBID 1RKE). (**B**) Superposition of the

structure of the RRM1 domain of raver1 in the Vt:RRM1 structure (light purple) versus the Vt:RRM1-3 (light blue) structure.

Supplementary Figure S4. Conservation of residues directing the vinculin-raver1 interaction

(**A**) Sequence-based alignment of the RRM1-3 domains of human (h), mouse (m), rat (r), and bovine (b) RRM1, human and mouse raver2 (RV2) RRM1, and human raver1 RRM2 and RRM3. The RNP1 and RNP2 consensus are indicated as well as the secondary structure elements. Residues involved in hydrogen bonding or electrostatic interactions are marked by with a triangle or sphere, respectively. (**B**) The Arg945 and Asp953 residues of human (h) vinculin that mediate its interaction with human raver1 are strictly conserved in mouse (m), chicken (c), porcine (p) and *Xenopus* (x) vinculin.

Supplementary Figure S5. Structural constraints provoked by the vinculin-raver1 interaction

Stereo superposition of full-length vinculin (Borgon et al., 2004; salmon) onto the vinculin tail domain in complex with raver1 (green and blue, respectively). The raver1 binding site is occluded by the 882-890 loop region of inactive vinculin, preventing the Tyr-92 region of raver1 to bind to vinculin in its native conformation.

Supplementary Figure S6. Comparison of the interface of RRM domain as seen in the SRPK1:ASF/SF2 and Vt:raver1 structures

(A) Stereo view of the interface of SRPK1 (green) and RRM2 of ASF/SF2 (slate blue) (Ngo et al., 2008). Important contact residues are shown as stick. (B) Superposition of the

RRM1 domain of raver1 (cyan) onto the RRM2 domain of ASF/SF2 (orange) reveals that while similar regions on the RRM domain are involved in the interface, the residues are distinct (shown in stick representation).

Supplementary Figure S7. Raver1 Binds *Vinculin* mRNA sequence 3089-3100 and Vt

We searched for a candidate for raver1 interacting mRNA in the mRNA sequences of the raver1 binding partners vinculin and α-actinin and identified *vinculin* mRNA 3089-3100 (UCAUGCAGUCUG). Shown are ITC analyses of binding of this RNA to the RRM1 motif of raver1 (ΔH, 41.2±1.4 kcal/mol; ΔS, 163 cal/mol).

Supplemental Figure S1

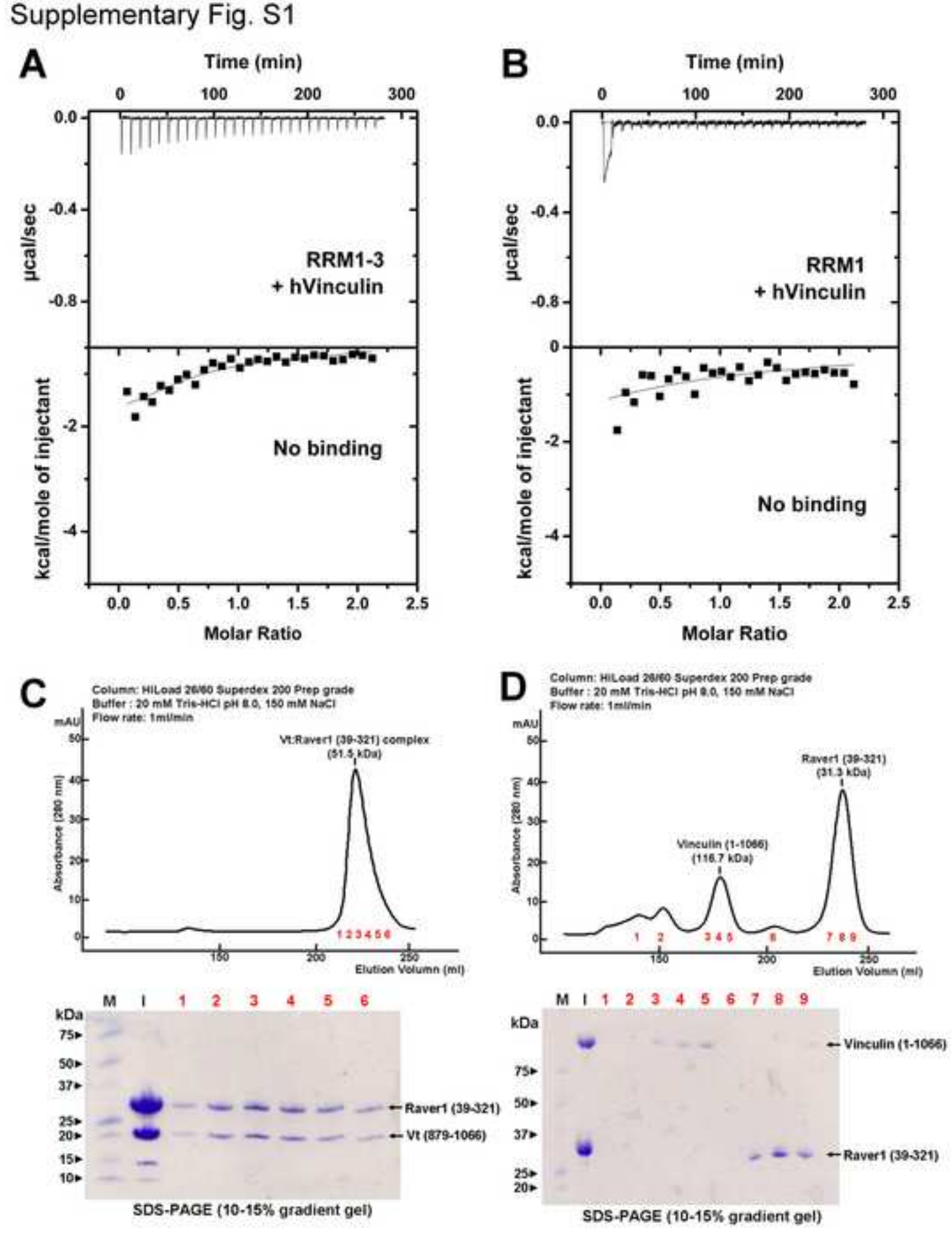

Supplemental Figure S2

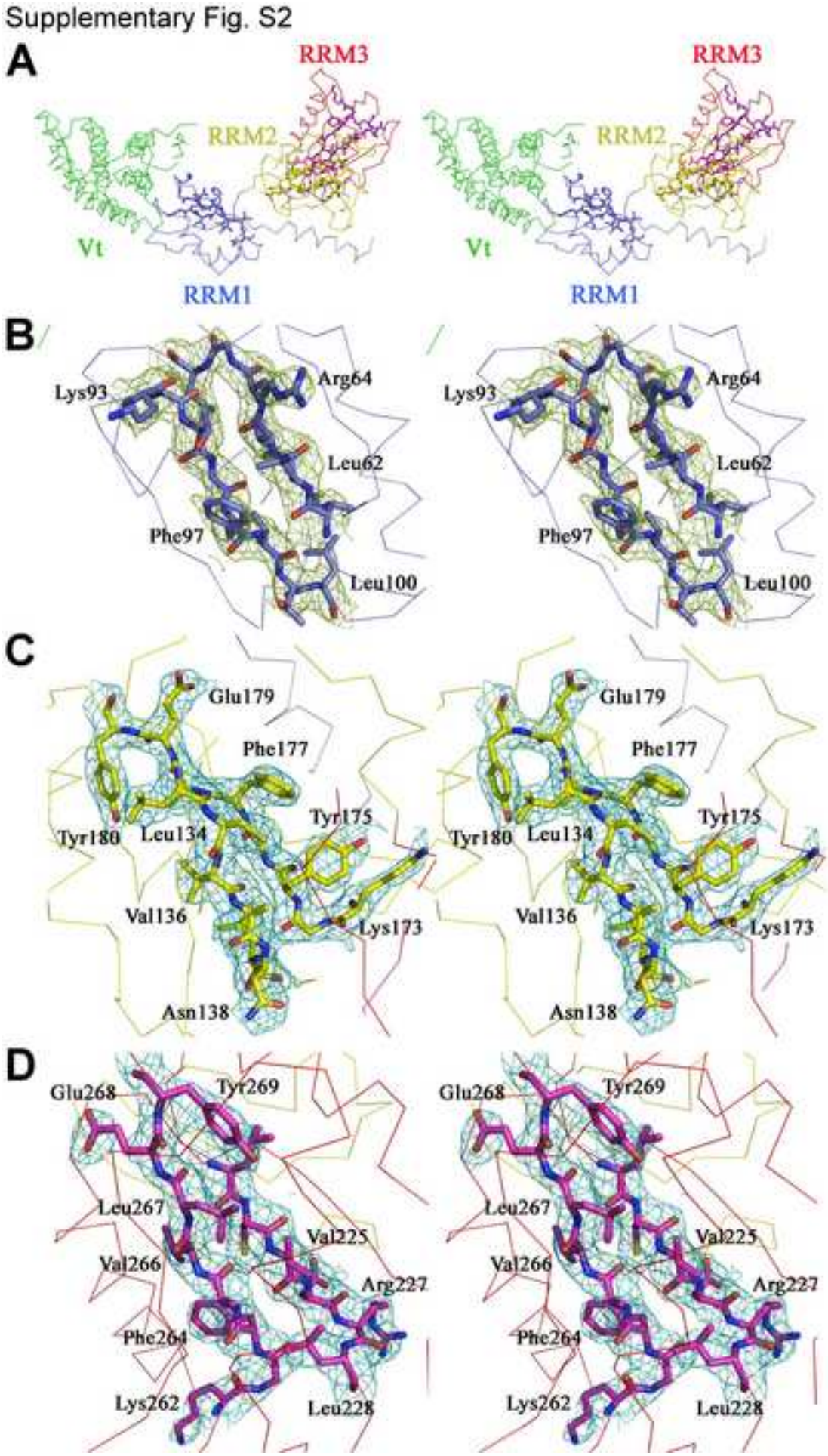

Supplemental Figure S3

Supplementary Fig. S3

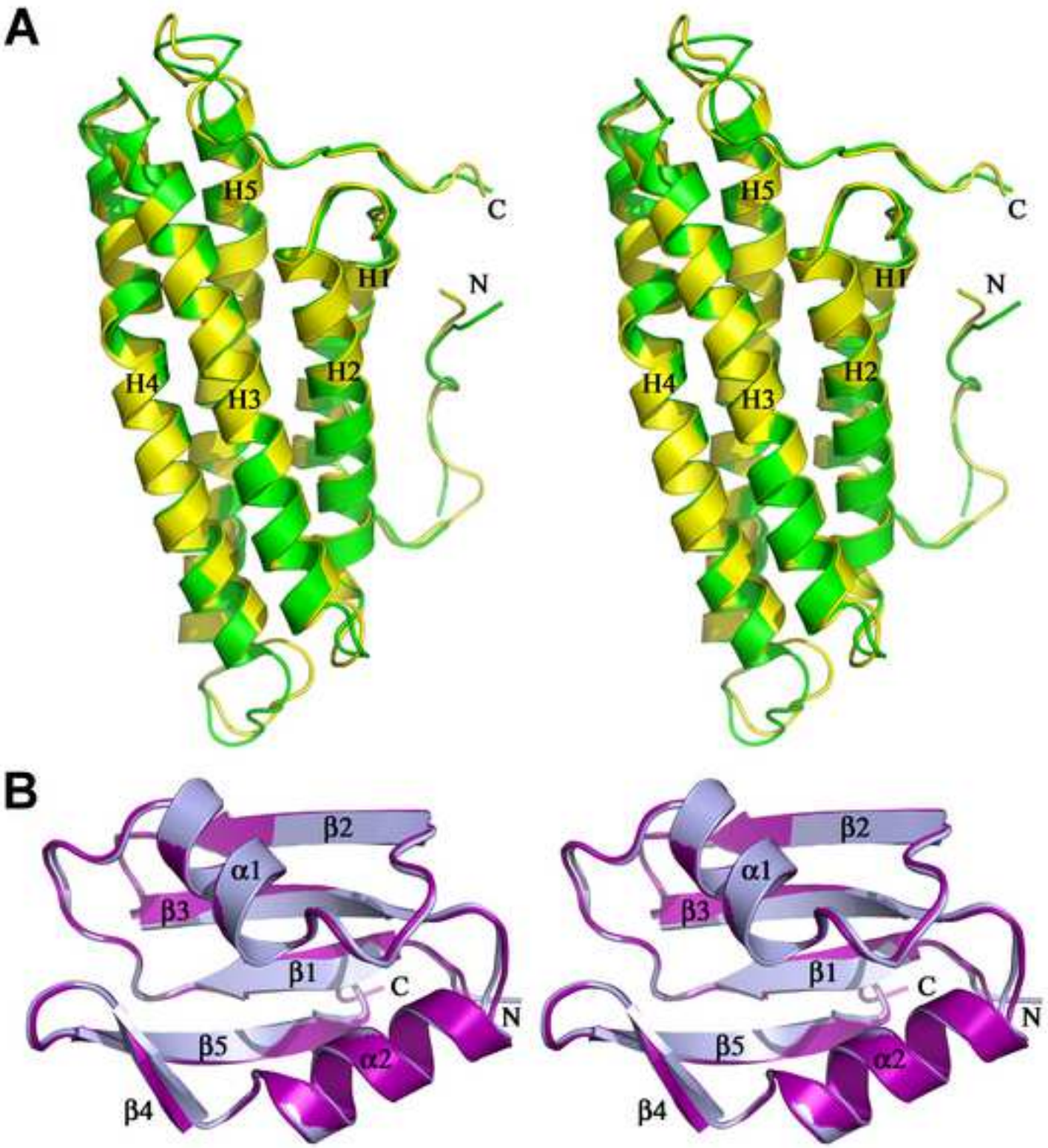

Supplemental Figure S4

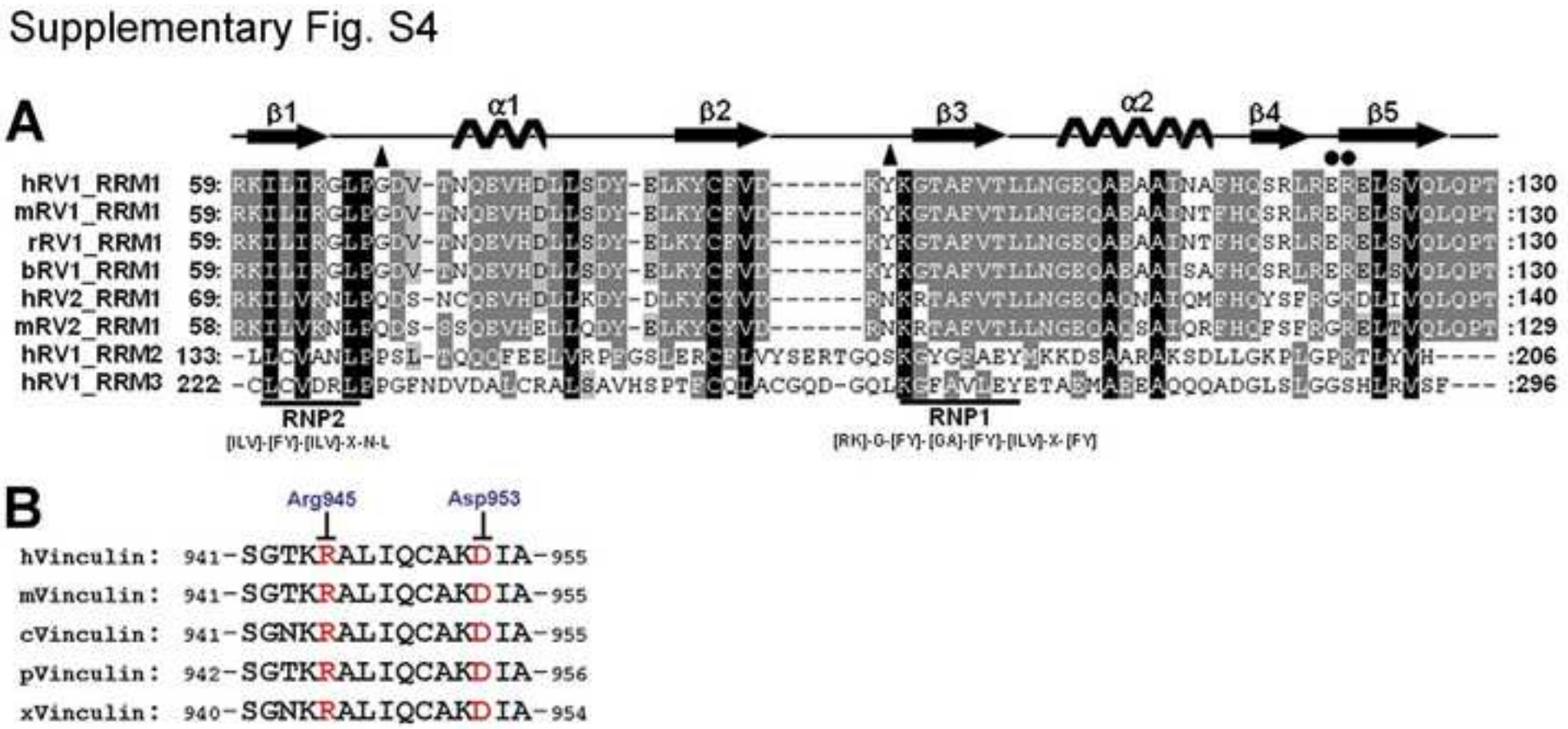

Supplemental Figure S5

Supplementary Fig. S5

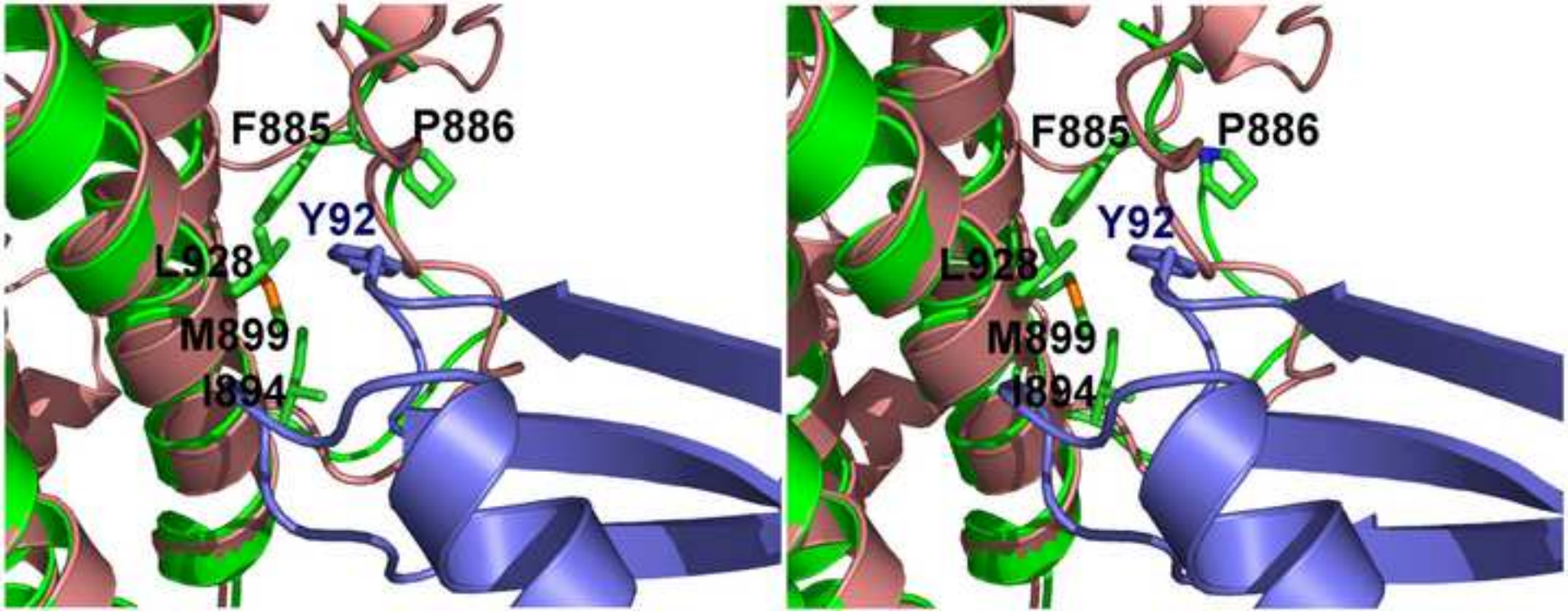

Supplemental Figure S6

Supplementary Fig. S6

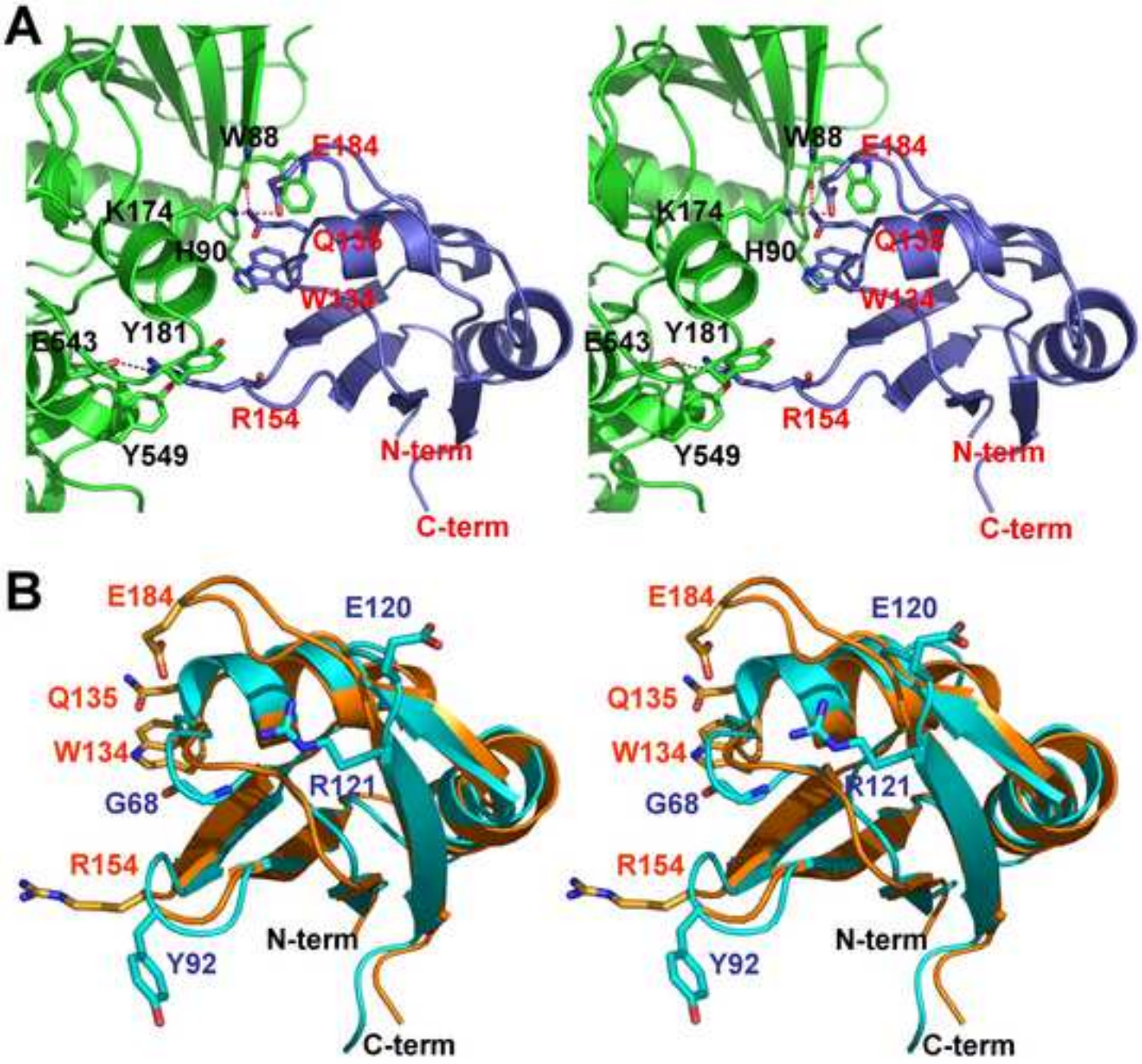

Supplementary Fig. S7